Footprints of past earthquakes revealed in the afterslip of the 2010 Mw 7.8 Mentawai tsunami earthquake

Feng, Lujia; Barbot, Sylvain; Hermawan, Iwan; Banerjee, Paramesh; Natawidjaja, Danny H.; Hill, Emma Mary

2016

Feng, L., Barbot, S., Hill, E. M., Hermawan, I., Banerjee, P., & Natawidjaja, D. H. (2016). Footprints of past earthquakes revealed in the afterslip of the 2010 Mw 7.8 Mentawai tsunami earthquake. Geophysical Research Letters, 43(18), 9518-9526.

https://hdl.handle.net/10356/86282

https://doi.org/10.1002/2016GL069870

AGU PUBLICATIONS

Geophysical Research Letters

RESEARCH LETTER
10.1002/2016GL069870

Key Points:
- Five years of afterslip following the 2010 M_w 7.8 Mentawai earthquake released postseismic moment equivalent to a M_w 7.6 earthquake
- The 2010 afterslip progressed downdip relative to the 2010 coseismic rupture
- Stress changes from the coseismic slip and afterslip of the 2007 M_w 8.4 Bengkulu sequence affected the evolution of the 2010 afterslip

Supporting Information:
- Supporting Information S1
- Movie S1
- Data Set S1
- Data Set S2

Correspondence to:
L. Feng,
lfeng@ntu.edu.sg

Citation:
Feng, L., S. Barbot, E. M. Hill, I. Hermawan, P. Banerjee, and D. H. Natawidjaja (2016), Footprints of past earthquakes revealed in the afterslip of the 2010 M_w 7.8 Mentawai tsunami earthquake, *Geophys. Res. Lett.*, *43*, 9518-9526, doi:10.1002/2016GL069870.

Received 6 JUN 2016
Accepted 5 SEP 2016
Accepted article online 9 SEP 2016
Published online 23 SEP 2016

Footprints of past earthquakes revealed in the afterslip of the 2010 M_w 7.8 Mentawai tsunami earthquake

Lujia Feng[1], Sylvain Barbot[1,2], Emma M. Hill[1,2], Iwan Hermawan[1], Paramesh Banerjee[1], and Danny H. Natawidjaja[3]

[1]Earth Observatory of Singapore, Nanyang Technological University, Singapore, [2]Asian School of the Environment, Nanyang Technological University, Singapore, [3]Research Center for Geotechnology, Indonesian Institute of Sciences (LIPI), Bandung, Indonesia

Abstract The 2010 M_w 7.8 Mentawai tsunami earthquake marks one of the first tsunami earthquakes to have postseismic deformation observed by geodetic instruments. The Sumatran GPS Array has recorded the postseismic deformation following this event continuously for >5 years. The spatiotemporal evolution of the postseismic deformation is well explained by velocity-strengthening frictional sliding on the Sunda megathrust. Our results show that the 2010 afterslip progressed downdip relative to the 2010 coseismic rupture. The southeastern portion of the afterslip region overlaps the area that slipped during the main shock and afterslip of the 2007 M_w 8.4 Bengkulu earthquake, while the northwestern portion slipped an area without recent large earthquakes. By incorporating pre-earthquake stress conditions into quasi-dynamic models, we demonstrate that the preceding cumulative slip from the 2007 sequence might have caused a ~0.1 MPa difference in pre-earthquake Coulomb stress between the southeastern and northwestern portions of the afterslip region.

1. Introduction

Tsunami earthquakes are a special class of earthquakes that generate a tsunami larger than one might expect for their measured seismic magnitude [*Kanamori*, 1972]. Since *Kanamori* [1972] first identified two tsunami earthquakes, only a handful of tsunami earthquakes have been identified by seismological methods in the modern instrumental period [*Okal and Newman*, 2001; *Lay and Bilek*, 2007]. Most of the identified tsunami earthquakes were shallow-dipping thrust events that occurred at shallow depths near the trench [*Lay and Bilek*, 2007], making it difficult to record them with land-based geodetic networks. However, due to the relatively close distance of the Sumatran GPS Array (SuGAr), the 2010 M_w 7.8 Mentawai tsunami earthquake [*Newman et al.*, 2011; *Lay et al.*, 2011; *Bilek et al.*, 2011; *Satake et al.*, 2013] became the first tsunami earthquake to be captured in great detail by continuous geodetic networks [*Hill et al.*, 2012]. The SuGAr recorded not only coseismic deformation but also rapid and substantial afterslip associated with the 2010 Mentawai event.

Afterslip following a tsunami earthquake has been rarely, if ever, documented by geodetic instruments, so this Mentawai event perhaps marks the first such observation and provides an unprecedented opportunity to study afterslip at shallow regions of subduction zones. Thus, one goal of this paper is to document the long-term postseismic deformation following the 2010 Mentawai event, derive a detailed spatiotemporal evolution history of the 2010 afterslip using quasi-dynamic afterslip models, and investigate fault frictional properties on the Sunda megathrust, as has been done in many other regions [e.g., *Johnson et al.*, 2006; *Perfettini and Avouac*, 2007; *Barbot et al.*, 2009].

The 2010 Mentawai earthquake was not a stand-alone event, unlike most other tsunami earthquakes. Instead, this 2010 event occurred as part of the uncompleted most recent cycle of large earthquakes on the Mentawai segment of the Sunda megathrust [*Sieh et al.*, 2008], closely related to several preceding large events in space and time (Figure 1). These preceding events include the 2007 M_w 8.4 Bengkulu earthquake and its M_w 7.9 and 7.0 aftershocks [e.g., *Konca et al.*, 2008; *Lubis et al.*, 2013; *Tsang*, 2016] and the 2008 M_w 7.2 North Pagai earthquake [*Collings et al.*, 2012]. They broke primarily the central portion of the Sunda megathrust at depths from 15 to 35 km [*Konca et al.*, 2008], while the 2010 coseismic slip was concentrated along a near-trench

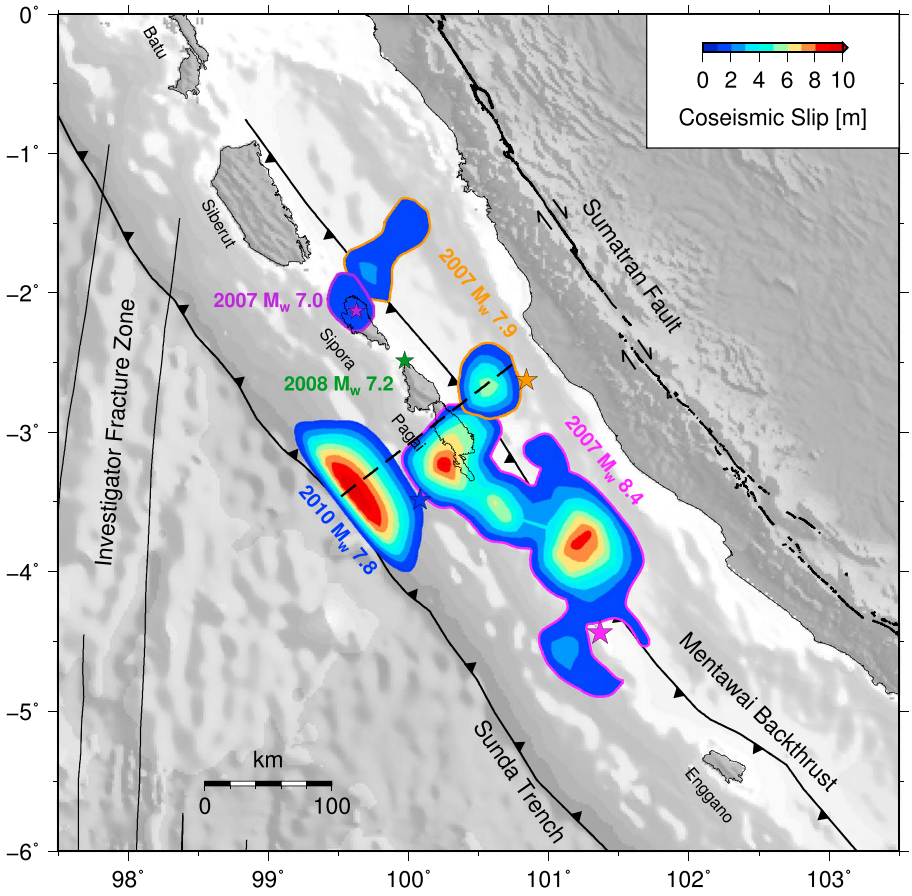

Figure 1. Map of recent $M_w > 7$ earthquakes in the Mentawai segment. Closed contours indicate areas of coseismic slip ≥1 m for the 2007 Bengkulu earthquake sequence [*Konca et al.*, 2008] and the 2010 Mentawai earthquake [*Hill et al.*, 2012]. Stars represent corresponding epicenters from the Advanced National Seismic System (ANSS) catalog. Black dashed line divides the Mentawai segment into two regions with a lot of slip released by the 2007 sequence in the southeast and no recent slip in the northwest.

portion of the Sunda megathrust at depths of <6 km, with peak slip of ~15 m [*Hill et al.*, 2012; *Yue et al.*, 2014, 2015]. Although the individual coseismic ruptures do not seem to overlap each other (Figure 1), their ensuing afterslip may well have invaded their own or neighboring coseismic rupture zones. *Tsang* [2016] show that the shallow afterslip of the 2007 main shock borders and overlaps the 2010 rupture zone and suggest that the cumulative stress changes from the main shock and afterslip may have advanced in time the shallow 2010 rupture.

If the preceding large events and their afterslip indeed impacted the 2010 coseismic rupture, it is natural to ask whether they also impacted the 2010 afterslip. Therefore, the other goal of this paper is to investigate the impact of past earthquakes on the 2010 afterslip. To achieve this goal, we compare two scenarios of stress-driven afterslip models: one without and the other with pre-earthquake stress conditions considered. Based on our results, we propose that the preceding large events may have left footprints in the stress field that influenced the afterslip evolution of the 2010 Mentawai earthquake.

2. Postseismic GPS Time Series

The postseismic deformation following the 2010 Mentawai earthquake was captured by 14 SuGAr stations on the Mentawai islands (Siberut, Sipora, North Pagai, and South Pagai) and west coast of Sumatra (Figures 2 and 3). In addition to the 2010 postseismic signal, the 14 stations were distracted by a panoply of other signals that included linear rates, seasonal signals, coseismic offsets, and postseismic decays associated with other earthquakes. In order to isolate the postseismic signal associated with the 2010 earthquake, we followed the

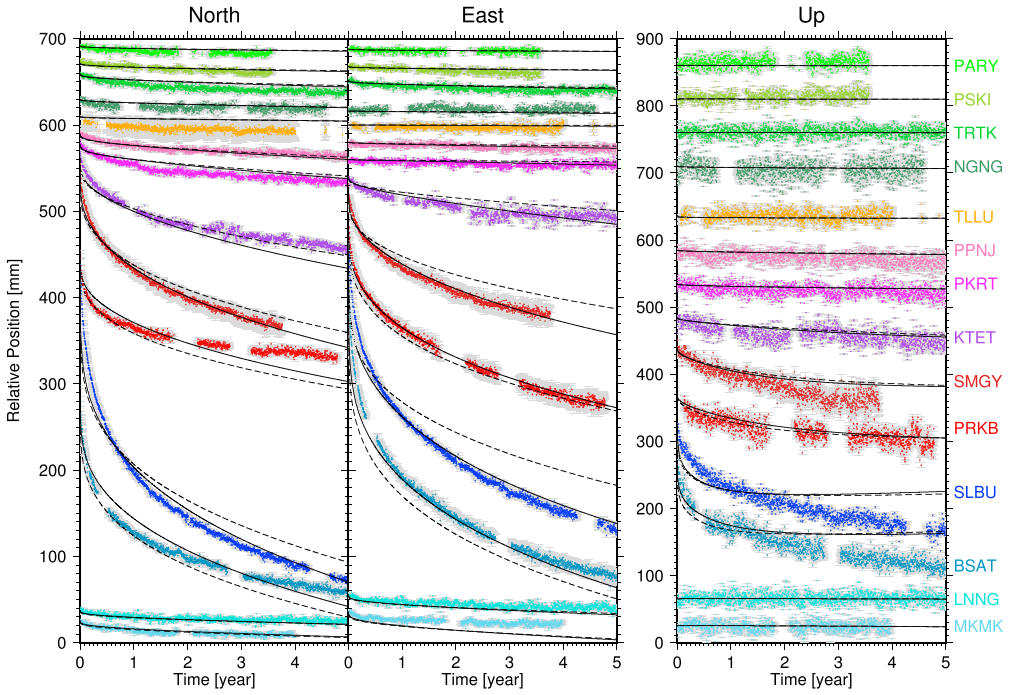

Figure 2. Postseismic time series of daily positions in the Sunda reference frame [*Altamimi et al.*, 2012] for the 2010 Mentawai earthquake. Dashed lines are modeled time series based on the best fit model of Scenario 1 (red star in Figure S7 in the supporting information). Solid lines are modeled time series based on the best fit model of Scenario 2 (red star in Figure 4). Time zero indicates the day of the 2010 event.

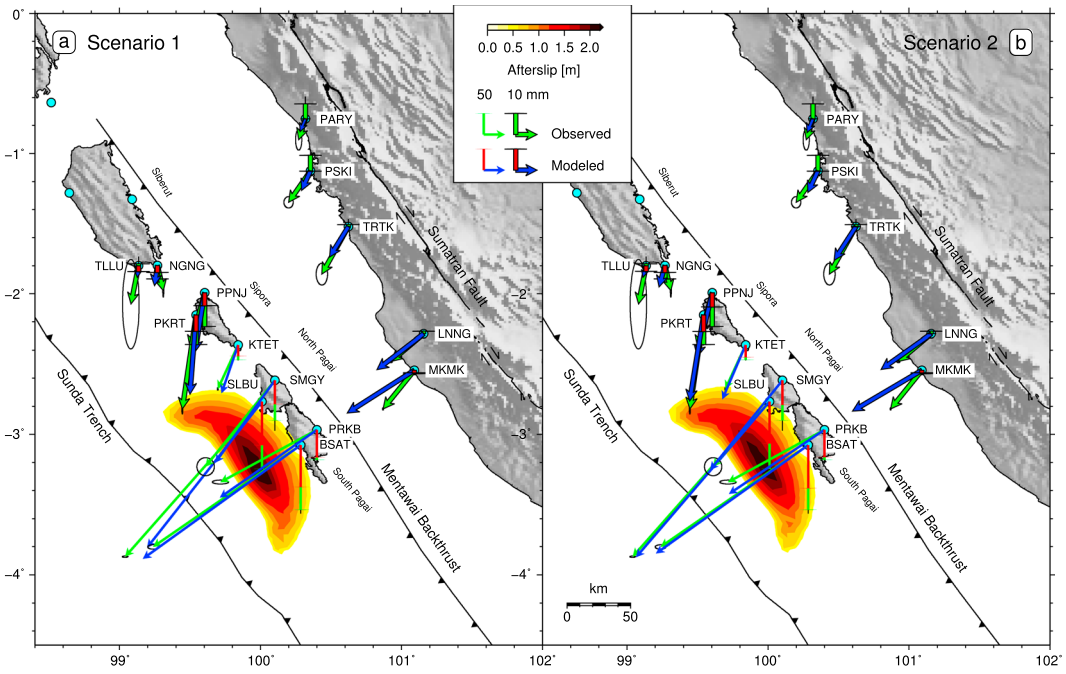

Figure 3. Observed (green) and modeled (blue and red) cumulative postseismic displacements of the 2010 Mentawai earthquake for the first 5 years. Note that two different vector scales are used. Error ellipses show 95% confidence level for the observed displacements. Contours indicate areas of 5 year cumulative afterslip ≥0.5 m for the best fit model of the two scenarios, respectively.

data processing and time series fitting procedures described in detail by *Feng et al.* [2015]. Simply speaking, we simultaneously fit all the known signals on the north, east, and vertical components of each station and then removed the distracting ones to obtain the 2010 postseismic signal alone.

The postseismic time series we obtained extend, with some data gaps, from immediately after the earthquake to mid-2014 for SMGY and PSKI, and to late 2015 or early 2016 for the remaining 12 stations (Figures 2 and S1 and Data Set S1). In the 5 year period from 25 October 2010 to 25 October 2015, the cumulative horizontal postseismic displacements at all stations either equaled or greatly exceeded horizontal coseismic displacements (Figure S2). The ratio of 5 year cumulative horizontal postseismic displacements to daily static coseismic estimates averages 1.4, while the ratio increases to 1.8 when compared to 1 s kinematic coseismic estimates. Note that kinematic horizontal coseismic estimates for this event are on average 30% smaller than static estimates [*Hill et al.*, 2012]. This discrepancy indicates that a significant fraction of postseismic deformation occurred rapidly within a day of the earthquake, which means we had to exclude the first-day postseismic deformation from the total postseismic estimation because the daily positions we used cannot capture motion happening within a day. Such exclusion likely causes the total postseismic deformation to be underestimated but should not affect its spatial pattern substantially. We can infer this because the horizontal postseismic motions continued mostly in the same trenchward direction as the coseismic motions, with the average change in azimuth less than 5° (Figure S2). Though small, the azimuth changes seem to indicate that the centroid of afterslip moment release is shifted slightly northwestward along strike relative to the centroid of coseismic moment release. This northwestward shift coincides with the northwestward propagation of the coseismic rupture [*Lay et al.*, 2011; *Hill et al.*, 2012].

The vertical postseismic motions also continued generally in the same direction as the coseismic verticals (Figure S2). Most coastal stations rose a little after the small (~5 mm) coseismic uplift, while most island stations switched from negligible coseismic vertical motion or small coseismic subsidence (up to ~6 cm at BSAT) to notably larger postseismic subsidence (up to ~16 cm in 5 years at SLBU). Interestingly, BSAT recorded the largest coseismic deformation, while SLBU recorded the largest postseismic deformation, which further confirms the northwestward along-strike shift of the slip centroid. The four closest stations on the Pagai islands (BSAT, SLBU, PRKB, and SMGY) experienced not only dramatically increased subsidence but also a decreased ratio of horizontal to vertical postseismic displacements, both suggesting the afterslip must have progressed downdip relative to the coseismic patch.

In sum, postseismic deformation in the first to fifth years (Data Set S2) contributes on average 60%, 16%, 11%, 7%, and 6% of the 5 year total. The postseismic velocities of the farthest stations (TLLU, NGNG, and all coastal stations) were reduced to less than 2 mm/yr within 1–3 years after the event, reaching a plateau when postseismic motion became trivial, while stations on the island of Sipora (PKRT, PPNJ, and KTET) have just reached or are close to reaching this plateau (Figure S3). In contrast, the four closest Pagai stations are still moving at 1.5–2.5 cm/yr trenchward and subsiding at 0.5–1 cm/yr, showing no sign of reaching the plateau yet (Figure S3).

3. Quasi-Dynamic Models of Stress-Driven Afterslip

Since the 2010 Mentawai earthquake was so shallow that the postseismic effect from viscoelastic relaxation is considered to be small, we model the postseismic evolution purely as a result of frictional afterslip on the Sunda megathrust. Such quasi-dynamic models reduce the large number of free parameters in kinematic models to only a few that have physical meanings and meanwhile avoid the spatial resolution issue of the shallow megathrust. This spatial resolution issue has been demonstrated by *Hill et al.* [2012] in kinematic coseismic models of this 2010 earthquake and further confirmed in our kinematic afterslip inversions using the principal component analysis-based inversion method (PCAIM) [*Kositsky and Avouac*, 2010] (Text S1). To illustrate the impact of past slip on the 2010 afterslip, we develop two scenarios of stress-driven afterslip models.

3.1. Scenario 1: Coseismic Stress-Driven Models

In the first scenario, afterslip is triggered by stress changes from coseismic slip and then evolves following a rate-strengthening friction law. Rate-strengthening friction laws simplify rate-and-state friction laws to steady-state cases, where the evolution of the state variable is neglected and friction depends only on rate, so that slip rate can be directly related to stress change. Such a direct link can be expressed as equation (1)

[*Rousset et al.*, 2012] in the form of a generalized version of the rate-strengthening friction law [*Rice et al.*, 2001; *Barbot et al.*, 2009].

$$V = 2V_0 \sinh \frac{\Delta\tau}{(a-b)\bar{\sigma}} \tag{1}$$

Here the slip rate of afterslip V is controlled by the shear-stress-related numerator $\Delta\tau$ and normal-stress-related denominator $(a-b)\bar{\sigma}$. $\Delta\tau$ is shear stress change. $\bar{\sigma}$ is effective normal stress with its change assumed to be negligible compared to $\bar{\sigma}$ itself, while a and b are frictional parameters. Because $(a-b)$ and $\bar{\sigma}$ cannot be separately determined, we fix $\bar{\sigma}$ to be 200 MPa (a representative value for 10 km depth [*Lapusta and Barbot*, 2012]), and explore the range of $(a-b)$. We also explore the range of V_0, which is the reference slip rate that controls the timescale of afterslip. Both $(a-b)$ and V_0 may vary spatially and temporally when local environments (such as sliding velocities, temperatures, and fluid pressures) change, but for the sake of simplicity, we assume $(a-b)$ and V_0 to be constant over time and uniform everywhere on the fault.

The initial value of $\Delta\tau$ is shear stress change induced by coseismic slip. The coseismic source model we use was derived from high-rate GPS coseismic offsets and tsunami data and established on a planar interface [*Hill et al.*, 2012]. The planar geometry is suitable for modeling shallow coseismic ruptures; however, a more realistic geometry is needed for modeling afterslip along deeper portions of the slab. Thus, we combine the shallow geometry in *Hill et al.* [2012] with the geometry of Slab1.0 [*Hayes et al.*, 2012], which controls slab geometry at ≥20 km depth, and we discretize the combined interface into 912 rectangular patches that have an along-strike length of ~11 km and an along-dip width varying from 4 to 10 km. On each patch, the coseismic stress change is calculated using the Okada dislocation model [*Okada*, 1992] by summing up each patch's individual contribution. While afterslip evolves, it induces additional postseismic stress that changes $\Delta\tau$. Slip evolution due to changing $\Delta\tau$ is simulated using an explicit time step procedure with a fifth-order accurate scheme. The rake direction of afterslip is parallel to the direction of instantaneous shear stress acting on each patch, with the exception that unrealistic landward slip is not allowed.

The implicit assumption of equation (1) is that the change in normal stress $\Delta\sigma$ from either coseismic slip or afterslip is negligible so that effective normal stress $\bar{\sigma}$ can be fixed to a constant value throughout the afterslip process, and $\Delta\tau$ alone represents the Coulomb stress change $\Delta\mathrm{CFF} = \Delta\tau - \mu_0\Delta\sigma$, where μ_0 is the friction coefficient at V_0.

3.2. Senario 2: Preseismic and Coseismic Stress-Driven Models

Scenario 2 is similar to Scenario 1 in almost all aspects except that afterslip is related to not only coseismic stress change but also pre-earthquake stress conditions. The pre-earthquake stress conditions, often ignored in previous afterslip studies [e.g., *Barbot et al.*, 2009], can be incorporated using pre-earthquake Coulomb stress CFF_0 that is defined as $(\tau_0 - \mu_0\bar{\sigma})$, where τ_0 is the pre-earthquake shear stress and $\bar{\sigma}$ is fixed at 200 MPa as in Scenario 1. We do not determine individual values for τ_0 and μ_0; instead, we explore the possible values for CFF_0. Therefore, equation (1) is modified to equation (2) following the derivation in *Chang et al.* [2013].

$$V = 2V_0 \left[\sinh \frac{\Delta\tau + \mathrm{CFF}_0}{(a-b)\bar{\sigma}} - \sinh \frac{\mathrm{CFF}_0}{(a-b)\bar{\sigma}}\right] \tag{2}$$

To investigate the impact of past slip, we divide our slab interface into two portions with the southeastern portion that slipped during past events and the northwestern portion that has not recently generated a large earthquake (dashed line in Figure 1). We use CFF_0(SE) and CFF_0(NW) to represent uniform CFF_0 for the southeastern and northwestern portions, respectively.

4. Results

In order to find the combination of parameters that best explains the postseismic time series, we used a simple grid search to explore a physically possible range of model parameters. For each set of parameters, we computed forward models and calculated the cost function, which is the root-mean-square (RMS) of the misfit between the observed and modeled daily time series for all three components.

For Scenario 1, we tested $(a-b)$ in a wide range from 5×10^{-5} to 10 and V_0 from 5×10^{-4} to 50 m/yr. Although the lowest misfit (3.44 m) was reached when $(a-b) = 5.0\times10^{-4}$ and $V_0 = 3.0\times10^{-3}$ m/yr, a strong trade-off existed between $(a-b)$ and V_0. Any $(a-b)$ from 4×10^{-4} to 8×10^{-4} could be paired with a V_0 between 1×10^{-3}

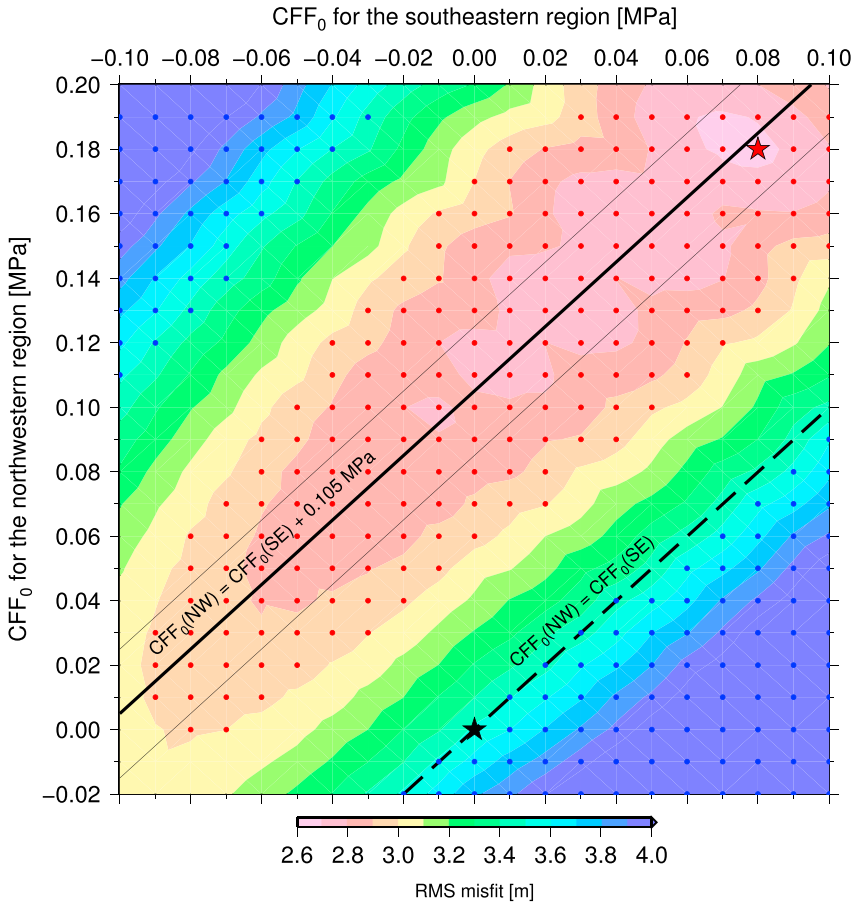

Figure 4. Contours of the RMS misfit for CFF_0(SE) and CFF_0(NW) in Scenario 2. $(a - b)\bar{\sigma}$ is fixed at 0.12 MPa and a V_0 that produces the lowest misfit is found for each CFF_0 pair (Figure S8). Red dots indicate models with misfit ≤3 m, while blue dots indicate models with misfit larger than the lowest misfit of Scenario 1 (3.44 m). Black star represents the model with zero CFF_0, equivalent to Scenario 1. Dashed line marks models for CFF_0(SE) = CFF_0(NW). Solid lines outline the low-misfit region. Red star represents the best fit model with its parameters summarized in Table S1.

and 1.3×10^{-2} to produce similarly small (<4 m) RMS misfits (Figure S7). Recall that we fixed $\bar{\sigma}$ at 200 MPa, so the range of $(a - b)$ corresponds to $(a - b)\bar{\sigma}$ ranging from 0.08 to 0.16 MPa. Although this range is an order of magnitude smaller than typical values of ~1 MPa derived from other studies [*Rollins et al.*, 2015], it is comparable to $(a - b)\bar{\sigma}$ derived for shallow depths [*Chang et al.*, 2013; *Johnson et al.*, 2006].

Despite the fact that Scenario 1 is oversimplified with only two free parameters, the best fit model can explain reasonably well the amplitude of GPS postseismic displacements (Figure 3a) and the postseismic time series of far-field stations (Figure 2). However, this model cannot fully explain the azimuth of the near-field postseismic displacements or the shape of the near-field postseismic time series.

For Scenario 2, to reduce the computation time, we fixed $(a - b)\bar{\sigma}$ at three values (0.10, 0.12, and 0.14 MPa) according to our results from Scenario 1 and then varied V_0 to search for the lowest misfit for every pair of CFF_0(SE) and CFF_0(NW). Figure 4 shows the lowest misfit contours when $(a - b)\bar{\sigma}$ is fixed at 0.12 MPa. Models that produced a low misft of <3 m all fall within the CFF_0(NW) > CFF_0(SE) quadrant, while models in the CFF_0(NW) ≤ CFF_0(SE) quadrant produced a misft even worse than the model without adding any CFF_0 (black star in Figure 4). Interestingly, the low-misfit contours (pink areas in Figure 4) indicate a constant difference (0.105 MPa) between CFF_0(SE) and CFF_0(NW) (solid lines in Figure 4). A similar constant difference of either 0.10 MPa or 0.11 MPa can be found in the misfit contours for $(a - b)\bar{\sigma} = 0.10$ MPa and $(a - b)\bar{\sigma} = 0.14$ MPa (Figures S9 and S10), but the location of the low-misfit region clearly shifts in the CFF_0 space for different $(a - b)\bar{\sigma}$ values. This shift means we cannot determine the absolute values of CFF_0(SE) and CFF_0(NW)

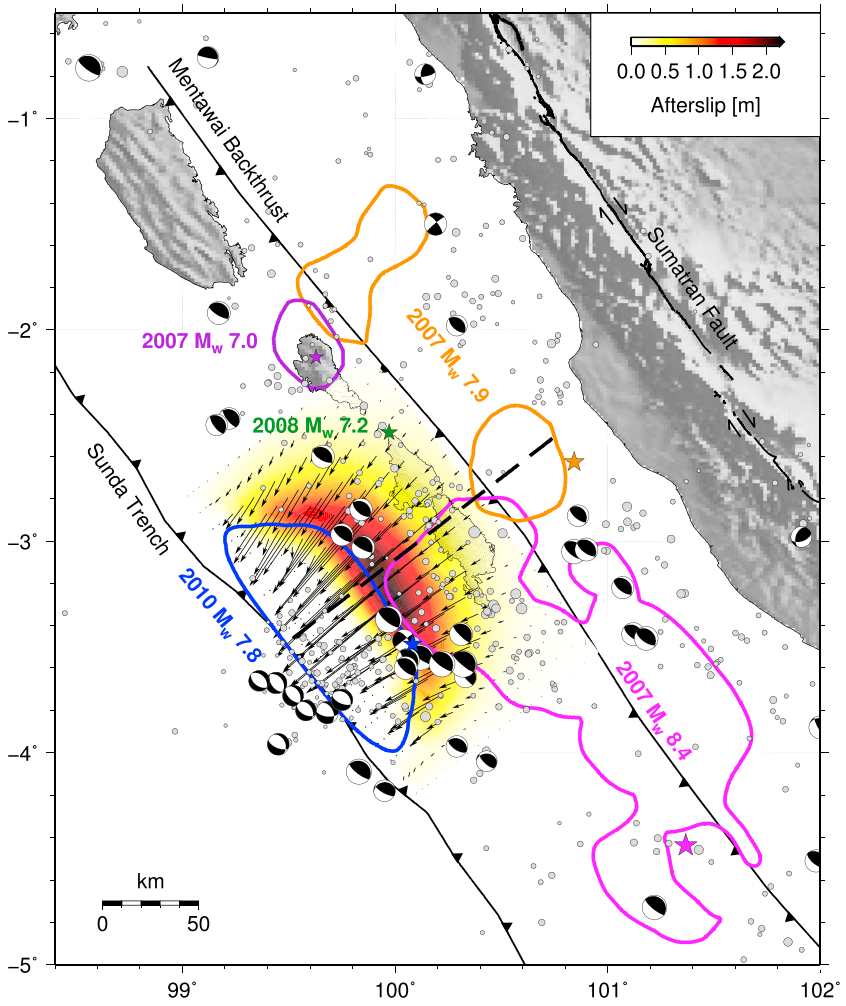

Figure 5. Five year cumulative afterslip of the 2010 Mentawai earthquake based on the best fit model shown in Figure 4. Gray circles indicate earthquakes recorded in the ANSS catalog during the 5 year afterslip period. Focal mechanisms for the 5 years are from the global centroid moment tensor catalog [*Ekström et al.*, 2012]. See Figure 1 for other features.

separately; however, the ~0.1 MPa less CFF_0 required for the southeastern portion seems to be robust for all the three $(a-b)\bar{\sigma}$ values.

In order to test if the constant difference is an artifact from the input coseismic model, we switched the preferred model in *Hill et al.* [2012] to a much rougher model and conducted the same procedures from Scenario 1 to Scenario 2. For Scenario 2, $(a-b)\bar{\sigma}$ was fixed at the best fit value (0.12 MPa) in Scenario 1. Even though using this rougher model in Scenario 2 increases misfits, the pattern of misfits in the CFF_0 space is similar to that derived from the preferred model, indicating a constant difference (0.07 MPa) between CFF_0(SE) and CFF_0(NW) (Figure S11). Hence, the constant difference seems to be a robust feature that stays when the coseismic model is changed.

We propose that the ~0.1 MPa difference is likely caused by the collective stress release from the main shock and afterslip of the 2007 Bengkulu earthquake and its numerous aftershocks before the 2010 Mentawai earthquake. Although we cannot completely exclude the possibility that the ~0.1 MPa difference is due to pre-2007 heterogeneous background stress, the pre-2007 interseismic coupling models seem to suggest the same degree of coupling for the two portions [*Prawirodirdjo et al.*, 2010] or less coupling in the northwestern portion [*Chlieh et al.*, 2008]. Either case could not explain the higher pre-earthquake stress required for the northwestern portion in our models. Furthermore, our additional tests show that the postseismic data do not favor strong along-strike variations in $(a-b)\bar{\sigma}$; thus, along-strike variations of frictional properties could not explain the constant difference either (Figure S14).

Compared to Scenario 1, the best fit model of Scenario 2 greatly improved the fits to the near-field postseismic horizontal time series with the misfit reduced to 2.68 m (Figures 2 and S15). The Scenario 2 model also better reproduced azimuth directions of the near-field GPS displacements (Figure 3b). However, the Scenario 2 model does not fit the far-field Sumatra mainland stations better than the Scenario 1 model, and both models poorly fit the vertical component of SLBU, BSAT, and SMGY. These misfits might be due to the uniform frictional properties we assumed or the viscoelastic effect we neglected in our models.

5. Discussion

Our results indicate that the 2010 afterslip occurred downdip of the 2010 coseismic rupture, with the main afterslip region in the depth range of 6 to 12 km (Figure 5 and Movie S1). The southeastern portion of the afterslip region partially overlaps the area that slipped during the main shock and afterslip of the 2007 M_w 8.4 Bengkulu earthquake [*Konca et al.*, 2008; *Tsang*, 2016]. The fact that the same area slipped during both the 2007 coseismic rupture and 2010 afterslip appears to contradict with the traditional asperity model in which persistent coseismic velocity-weakening asperities are surrounded by aseismic velocity-strengthening creep regions [*Lay and Kanamori*, 1980]. A similar contradiction was found in the afterslip following the 2011 Tohoku-oki earthquake [*Johnson et al.*, 2012]. However, the apparent contradiction could be reconciled if the overlapping area represents a conditionally-stable region so that it could participate in both the 2007 coseismic slip and 2010 afterslip processes [e.g., *Lay et al.*, 2012].

Over the 5 years following the 2010 Mentawai earthquake, afterslip reached a maximum slip of ~2.2 m and released postseismic moment of $\sim 3 \times 10^{20}$ N m. The postseismic moment release is equivalent to a M_w 7.6 earthquake and 40% of the coseismic moment release.

Aftershocks following the 2010 Mentawai earthquake occurred in two main clusters (Figure 5). The shallower cluster features normal faulting in the subducting slab, while the deeper cluster comprises mainly thrust faulting along the margins of the 2007 and 2010 coseismic ruptures [*Yue et al.*, 2014]. According to the Advanced National Seismic System (ANSS) composite catalog, ~100 aftershocks ($4.0 \leq M_w \leq 6.3$) occurred within the afterslip region during the 5 year afterslip period. Their summed seismic moment amounts to $\sim 1 \times 10^{19}$ N m, equivalent to a M_w 6.6 earthquake. Thus, the seismic moment release accounts for only ~3% of the moment release by the 2010 afterslip, suggesting that the 2010 afterslip is mainly aseismic, similar to the 2005 M_w 8.6 Nias-Simeulue [*Hsu et al.*, 2006] and 2007 M_w 8.4 Bengkulu earthquakes [*Lubis et al.*, 2013].

6. Conclusions

With our quasi-dynamic models, we show that the southeastern portion of the 2010 afterslip region has ~0.1 MPa less pre-earthquake Coulomb stress than the northwestern portion. We propose that this difference in pre-earthquake Coulomb stress may have been caused by the main shock, aftershocks, and afterslip of the 2007 Bengkulu sequence.

Acknowledgments
SuGAr GPS data are available for download from ftp://eos.ntu.edu.sg/SugarData with a latency of 3 months. Figures were made using the Generic Mapping Tools (GMT) [*Wessel et al.*, 2013]. We are grateful to the many scientists and field technicians who have spent time in rugged field and ocean conditions to keep the SuGAr network in operation. These include Jeffrey Encillo, Imam Suprihanto, Dudi Prayudi, and Bambang Suwargadi. We appreciate Louisa Tsang for her help with PCAIM. We are grateful to Jean-Philippe Avouac and Ya-Ju Hsu for useful discussions. We thank two reviewers, Roland Bürgmann and Romain Jolivet, for their constructive comments that improved the paper. We thank Pavel Adamek for giving invaluable linguistic suggestions. This research was supported by an NTU startup grant to E.M.H., by the National Research Foundation Singapore under its Singapore NRF Fellowship scheme (National Research Fellow Award NRF-NRFF2010-064 to E.M.H. and NRF-NRFF2013-04 to S.B.), and by the Earth Observatory of Singapore via its funding from the National Research Foundation Singapore and the Singapore Ministry of Education under the Research Centres of Excellence initiative. This work is Earth Observatory of Singapore contribution number 117.

References

Altamimi, Z., L. Métivier, and X. Collilieux (2012), ITRF2008 plate motion model, *J. Geophys. Res.*, *117*, B07402, doi:10.1029/2011JB008930.

Barbot, S., Y. Fialko, and Y. Bock (2009), Postseismic deformation due to the M_w 6.0 2004 Parkfield earthquake: Stress-driven creep on a fault with spatially variable rate-and-state friction parameters, *J. Geophys. Res.*, *114*, B07405, doi:10.1029/2008JB005748.

Bilek, S. L., E. R. Engdahl, H. R. DeShon, and M. E. Hariri (2011), The 25 October 2010 Sumatra tsunami earthquake: Slip in a slow patch, *Geophys. Res. Lett.*, *38*, L14306, doi:10.1029/2011GL047864.

Chang, S.-H., J.-P. Avouac, S. Barbot, and J.-C. Lee (2013), Spatially variable fault friction derived from dynamic modeling of aseismic afterslip due to the 2004 Parkfield earthquake, *J. Geophys. Res. Solid Earth*, *118*, 3431–3447, doi:10.1002/jgrb.50231.

Chlieh, M., J.-P. Avouac, K. Sieh, D. H. Natawidjaja, and J. Galetzka (2008), Heterogeneous coupling of the Sumatran megathrust constrained by geodetic and paleogeodetic measurements, *J. Geophys. Res.*, *113*, B05305, doi:10.1029/2007JB004981.

Collings, R., D. Lange, A. Rietbrock, F. Tilmann, D. Natawidjaja, B. Suwargadi, M. Miller, and J. Saul (2012), Structure and seismogenic properties of the Mentawai segment of the Sumatra subduction zone revealed by local earthquake traveltime tomography, *J. Geophys. Res.*, *117*, B01312, doi:10.1029/2011JB008469.

Ekström, G., M. Nettles, and A. M. Dziewoński (2012), The global CMT project 2004–2010: Centroid-moment tensors for 13,017 earthquakes, *Phys. Earth Planet. Inter.*, *200-201*, 1–9, doi:10.1016/j.pepi.2012.04.002.

Feng, L., E. M. Hill, P. Banerjee, I. Hermawan, L. L. H. Tsang, D. H. Natawidjaja, B. W. Suwargadi, and K. Sieh (2015), A unified GPS-based earthquake catalog for the Sumatran plate boundary between 2002 and 2013, *J. Geophys. Res. Solid Earth*, *120*, 3566–3598, doi:10.1002/2014JB011661.

Hayes, G. P., D. J. Wald, and R. L. Johnson (2012), Slab1.0: A three-dimensional model of global subduction zone geometries, *J. Geophys. Res.*, *117*, B01302, doi:10.1029/2011JB008524.

Hill, E. M., et al. (2012), The 2010 M_w 7.8 Mentawai earthquake: Very shallow source of a rare tsunami earthquake determined from tsunami field survey and near-field GPS data, *J. Geophys. Res.*, *117*, B06402, doi:10.1029/2012JB009159.

Hsu, Y.-J., M. Simons, J.-P. Avouac, J. Galetzka, K. Sieh, M. Chlieh, D. H. Natawidjaja, L. Prawirodirdjo, and Y. Bock (2006), Frictional afterslip following the 2005 Nias-Simeulue earthquake, Sumatra, *Science*, *312*(5782), 1921–1926, doi:10.1126/science.1126960.

Johnson, K. M., R. Bürgmann, and K. Larson (2006), Frictional properties on the San Andreas fault near Parkfield, California, inferred from models of afterslip following the 2004 earthquake, *Bull. Seismol. Soc. Am.*, *96*(4B), S321–S338, doi:10.1785/0120050808.

Johnson, K. M., J. Fukuda, and P. Segall (2012), Challenging the rate-state asperity model: Afterslip following the 2011 M9 Tohoku-oki, Japan, earthquake, *Geophys. Res. Lett.*, *39*, L20302, doi:10.1029/2012GL052901.

Kanamori, H. (1972), Mechanism of tsunami earthquakes, *Phys. Earth Planet. Inter.*, *6*(5), 346–359, doi:10.1016/0031-9201(72)90058-1.

Konca, A. O., et al. (2008), Partial rupture of a locked patch of the Sumatra megathrust during the 2007 earthquake sequence, *Nature*, *456*(7222), 631–635, doi:10.1038/nature07572.

Kositsky, A. P., and J.-P. Avouac (2010), Inverting geodetic time series with a principal component analysis-based inversion method, *J. Geophys. Res.*, *115*, B03401, doi:10.1029/2009JB006535.

Lapusta, N., and S. Barbot (2012), Models of earthquakes and aseismic slip based on laboratory-derived rate-and-state friction laws, in *The Mechanics of Faulting: From Laboratory to Real Earthquakes*, chap. 6, edited by A. Bizzarri and H. S. Bhat, pp. 153–207, Research Signpost, Kerala, India.

Lay, T., and S. Bilek (2007), Anomalous earthquake ruptures at shallow depths on subduction zone megathrusts, in *The Seismogenic Zone of Subduction Thrust Faults*, chap. 15, edited by T. H. Dixon and J. C. Moore, pp. 476–511, Columbia Univ. Press, New York.

Lay, T., and H. Kanamori (1980), An asperity model of large earthquake sequences, in *Earthquake Prediction: An International Review*, vol. 4, edited by D. W. Simpson and P. G. Richards, pp. 579–592, AGU, Washington, D. C., doi:10.1029/ME004p0579.

Lay, T., C. J. Ammon, H. Kanamori, Y. Yamazaki, K. F. Cheung, and A. R. Hutko (2011), The 25 October 2010 Mentawai tsunami earthquake (M_w 7.8) and the tsunami hazard presented by shallow megathrust ruptures, *Geophys. Res. Lett.*, *38*, L06302, doi:10.1029/2010GL046552.

Lay, T., H. Kanamori, C. J. Ammon, K. D. Koper, A. R. Hutko, L. Ye, H. Yue, and T. M. Rushing (2012), Depth-varying rupture properties of subduction zone megathrust faults, *J. Geophys. Res.*, *117*, B04311, doi:10.1029/2011JB009133.

Lubis, A. M., A. Hashima, and T. Sato (2013), Analysis of afterslip distribution following the 2007 September 12 southern Sumatra earthquake using poroelastic and viscoelastic media, *Geophys. J. Int.*, *192*(1), 18–37, doi:10.1093/gji/ggs020.

Newman, A. V., G. Hayes, Y. Wei, and J. Convers (2011), The 25 October 2010 Mentawai tsunami earthquake, from real-time discriminants, finite-fault rupture, and tsunami excitation, *Geophys. Res. Lett.*, *38*, L05302, doi:10.1029/2010GL046498.

Okada, Y. (1992), Internal deformation due to shear and tensile faults in a half-space, *Bull. Seismol. Soc. Am.*, *82*(2), 1018–1040.

Okal, E. A., and A. V. Newman (2001), Tsunami earthquakes: The quest for a regional signal, *Phys. Earth Planet. Inter.*, *124*(1–2), 45–70, doi:10.1016/S0031-9201(01)00187-X.

Perfettini, H., and J.-P. Avouac (2007), Modeling afterslip and aftershocks following the 1992 Landers earthquake, *J. Geophys. Res.*, *112*, B07409, doi:10.1029/2006JB004399.

Prawirodirdjo, L., R. McCaffrey, C. D. Chadwell, Y. Bock, and C. Subarya (2010), Geodetic observations of an earthquake cycle at the Sumatra subduction zone: Role of interseismic strain segmentation, *J. Geophys. Res.*, *115*, B03414, doi:10.1029/2008JB006139.

Rice, J. R., N. Lapusta, and K. Ranjith (2001), Rate and state dependent friction and the stability of sliding between elastically deformable solids, *J. Mech. Phys. Solids*, *49*(9), 1865–1898, doi:10.1016/S0022-5096(01)00042-4.

Rollins, C., S. Barbot, and J.-P. Avouac (2015), Postseismic deformation following the 2010 M = 7.2 El Mayor-Cucapah earthquake: Observations, kinematic inversions, and dynamic models, *Pure Appl. Geophys.*, *172*(5), 1305–1358, doi:10.1007/s00024-014-1005-6.

Rousset, B., S. Barbot, J.-P. Avouac, and Y.-J. Hsu (2012), Postseismic deformation following the 1999 Chi-Chi earthquake, Taiwan: Implication for lower-crust rheology, *J. Geophys. Res.*, *117*, B12405, doi:10.1029/2012JB009571.

Satake, K., Y. Nishimura, P. S. Putra, A. R. Gusman, H. Sunendar, Y. Fujii, Y. Tanioka, H. Latief, and E. Yulianto (2013), Tsunami source of the 2010 Mentawai, Indonesia earthquake inferred from tsunami field survey and waveform modeling, *Pure Appl. Geophys.*, *170*(9), 1567–1582, doi:10.1007/s00024-012-0536-y.

Sieh, K., et al. (2008), Earthquake supercycles inferred from sea-level changes recorded in the corals of West Sumatra, *Science*, *322*(5908), 1674–1678, doi:10.1126/science.1163589.

Tsang, L. L. H. (2016), Characterizing the spectrum of slip behavior at the Sumatran subduction zone with long-term geodetic records, PhD thesis, Nanyang Technological Univ., Singapore. [Available at http://hdl.handle.net/10356/66292, accessed 2016-03-23.]

Wessel, P., W. H. F. Smith, R. Scharroo, J. Luis, and F. Wobbe (2013), Generic mapping tools: Improved version released, *Eos Trans. AGU*, *94*(45), 409–410, doi:10.1002/2013EO450001.

Yue, H., T. Lay, L. Rivera, Y. Bai, Y. Yamazaki, K. F. Cheung, E. M. Hill, K. Sieh, W. Kongko, and A. Muhari (2014), Rupture process of the 2010 M_w 7.8 Mentawai tsunami earthquake from joint inversion of near-field hr-GPS and teleseismic body wave recordings constrained by tsunami observations, *J. Geophys. Res. Solid Earth*, *119*(7), 5574–5593, doi:10.1002/2014JB011082.

Yue, H., T. Lay, L. Li, Y. Yamazaki, K. F. Cheung, L. Rivera, E. M. Hill, K. Sieh, W. Kongko, and A. Muhari (2015), Validation of linearity assumptions for using tsunami waveforms in joint inversion of kinematic rupture models: Application to the 2010 Mentawai M_w 7.8 tsunami earthquake, *J. Geophys. Res. Solid Earth*, *120*, 1728–1747, doi:10.1002/2014JB011721.